Wiley
International Journal of Chemical Engineering
Volume 2025, Article ID 2208949, 10 pages
https://doi.org/10.1155/ijce/2208949

WILEY

Research Article

Thermal Decomposition Behavior and Characterization of Automotive Paint Sludge

Pfulwani Kalani,[1] Ines Oliver,[2] Julia Molto-Berenguer,[2] Juan A. Conesa,[2] Litha Yapi,[3] Zuko Nofemele,[4] and Athi-Enkosi Mavukwana[1]

[1]*Department of Chemical and Materials Engineering, University of South Africa (UNISA), Roodepoort, Gauteng, South Africa*
[2]*Institute of Chemical Process Engineering, University of Alicante, Alicante, Spain*
[3]*Department of Chemical Engineering, University of Pretoria, Pretoria, Gauteng, South Africa*
[4]*Process Department, Volkswagen Group South Africa Pty Ltd, Kariega, Eastern Cape, South Africa*

Correspondence should be addressed to Athi-Enkosi Mavukwana; mavukae@unisa.ac.za

Received 10 April 2025; Revised 17 October 2025; Accepted 22 October 2025

Academic Editor: Arnab Biswas

Automotive paint sludge (APS) is a ubiquitous, recalcitrant waste product of the vehicle manufacturing process. The potential of APS for energy and chemical production via pyrolysis and gasification is undermined by the absence of methodologically consistent, cross-stream physicochemical characterization. This impedes process design for the valorization of APS. This work aims to rectify that by presenting a direct physicochemical characterization and thermogravimetric comparison of five APS types: electrocoat, phosphate coat, primer, base coat, and clear coat. Thermogravimetric (TGA/DTG) experiments were conducted at three heating rates, i.e., 5, 10, and 20°C/min, under both nitrogen and air atmospheres. The study revealed that the decomposition of APS occurs in three distinct stages. The first stage involves the removal of moisture and the release of volatile organic compounds (VOCs), occurring at temperatures ranging from 30°C to 220°C. The second stage, which occurs at approximately 220°C–550°C, exhibits a further subdivision profile comprising two subsections. This entails the devolatilization stage, which occurs between 200°C and 380°C. Subsequent to this, the cracking of resins, heavy hydrocarbons, and the formation of char occur at temperatures ranging from 380°C to 550°C. The third and final stage occurs at a range of 550°C–800°C, accounts for the least mass loss, and is characterized by the carbonization and decomposition of inorganic compounds. In this work, we have established temperature intervals for drying/VOC removal, VOC recovery, and secondary cracking/carbonization, providing comparative evidence to optimize APS-to-energy conversion.

Keywords: automotive paint sludge (APS); pyrolysis; reaction kinetics; thermogravimetric analysis (TGA/DTG)

1. Introduction

Finite fossil-fuel constraints and rising waste generation sharpen the need to recover value from inevitable industrial waste effluents [1, 2]. Among these, automotive paint sludge (APS), which is the overspray and capture residue from vehicle coating lines, accumulates at several tons per year and is commonly landfilled due to its organic load, solvents, pigments, and metals [3–7]. Redirecting APS to thermochemical valorization could reduce disposal liabilities while supplying fuels and carbonaceous products [8].

Industrial paint shops generate multiple, distinct paint sludge streams depending on capture and treatment methods, rather than a single homogenous APS stream. For instance, water-wash or wet scrubber booth sludge, dry-booth filter cakes, chemically detackified booth–water sludges, downstream dissolved air flotation (DAF)/clarifier paint sludges, and housekeeping or floor overspray residue. This is particularly pronounced for automotive industrial lines using wet as opposed to dry booth capture and associated handling [7]. These streams differ predominantly in the binder systems used: acrylics,

polyesters, epoxies, or polyurethanes. Furthermore, the difference is also characterized by whether the paints are solvent-borne or water-borne, as well as in additive or pigment packages used, i.e., titanium oxide (TiO_2) or iron oxides [3, 4].

These compositional differences are used to control volatile organic compound (VOC) release behavior, devolatilization temperature ranges, char yields/reactivity, and the speciation of evolved gases/oils during thermal conversion. Therefore, they invariably will shift kinetic parameters and optimal operating windows for pyrolysis or gasification [5]. Inorganics or ceramics common in APS, such as alumina (Al_2O_3), silica (SiO_2), calcium oxide (CaO), titanium oxide (TiO_2) or iron oxides, may further catalyze cracking or tar reduction. They may even alter the char gasification reactivity, thereby reinforcing that stream characteristics of the APS are pivotal to the potential end use of the valorization exercise [7]. Treating APS as a single feed therefore risks suboptimal designs: process development should resolve stream-level kinetics and ash chemistry rather than aggregate them [9].

Prior studies typically pool multiple APS sources into a single composite feed or report single-stream results that are not directly comparable due to differing heating rates, particle sizes, or atmospheres [5, 6, 9–12]. This report focuses on studying these sludges comparatively and prioritizes assessing how each sludge can be recovered with thermal treatment technologies [8].

Thermogravimetric studies on paint wastes show consistent trends. Resin and plasticizer choices shift derivative thermogravimetric (DTG) peak temperatures. A higher fraction of the solvent or other light ends increases mass loss at low temperature. Inorganics and ash can catalyze secondary cracking, making the remaining char easier to gasify. Pigments and metals are likely to generate precursors that later form nitrogen oxides and sulfur oxides (NOx and SOx) during the oxidation process. The process gas also matters. Nitrogen, oxidizing, and carbon dioxide–rich atmospheres give different apparent activation energies and char structures [8, 13, 14].

This study systematically compares the thermal decomposition behavior of five APS streams produced along an automotive coating line. Thermogravimetric analysis (TGA/DTG) at multiple heating rates and under different atmospheres is used to extract kinetic parameters and identify characteristic devolatilization regions for each stream [15]. By testing all streams under identical conditions, the study links stream composition (organic versus inorganic content, solvent fraction, and pigment or metal levels) to char yield, reactivity, and the gases and oils produced. These links then identify, for each APS, suitable temperatures, residence times, and atmospheres for pyrolysis and gasification.

Across five APS streams, TGA/DTG measurements yield kinetic parameters linked to composition, quantifying how the atmosphere and heating rate shape devolatilization, char yield, and reactivity. The results are distilled into practical guidance on temperature windows, residence times, expected oil and gas outputs, and likely emission precursors, enabling process decisions grounded in stream-level measurements rather than averages.

2. Methodology

2.1. Materials. In this work, five APS samples were tested for pyrolytic and oxidative decomposition. The samples used for this test were donated by a large car manufacturer in South Africa and were taken from various stages of production processes and contained about 70% (wt) moisture. The five sludge samples are electrocoat, primer coat, base coat, clear coat, and phosphate sludge. The samples were collected by personnel from the manufacturing company, appropriately packaged, and subsequently shipped to the university. Safety Data Sheets (SDSs) for all samples were provided by the manufacturer. Given that the materials are classified as hazardous, all procedures were conducted in accordance with the Occupational Health and Safety (OHS) Act and the Regulations for Hazardous Chemical Agents, as well as the university's internal OHS protocols. Before the test, the sample was dried for 36 h at 102°C in an oven dryer. The samples were milled using a planetary ball mill (Retsch PM100, Biometa S.A., Spain) supplied by the Department of Chemical Engineering, University of Alicante. The milled material was subsequently sieved, and fractions with particle diameters smaller than 180 μm were selected for the thermal treatment experiments. Each milling cycle was set to four minutes per sample and repeated as necessary until the desired particle size (< 180 μm) was achieved.

2.2. Equipment. A PerkinElmer TGA 4000 was used to study the thermal decomposition of APS under a nitrogen or air atmosphere of a total flow rate of 100 mL/min and three different heating rates of 5, 10, and 20°C/min, heating the samples from 30°C to 800°C. The system was purged with nitrogen at a flow rate of 40 mL/min. A 10 ± 1 mg sample was used to avoid intraparticle heat transfer and ensure kinetic control of the process by reducing the occurrence of secondary vapor–solid interactions [16].

The ultimate analysis of APS was measured using a Thermo Scientific CHNS Elemental analyzer. The chemical composition and mineral composition were characterized by using both the inductively coupled mass spectrometer (ICP-MS, by Agilent) and the X-ray fluorescence spectrometer (by PANalytical). The HHV was determined using the IKA Werke C5003 bomb calorimeter. The Technical Research Services, University of Alicante, Spain, provided the characterization equipment.

2.3. Replicates, Repeatability, and Uncertainty Reporting. For each sludge type (electrocoat, primer, base, clear, and phosphate), one TGA run was conducted at each heating rate (5, 10, and 20°C·min^{-1}) under N_2 or air on a PerkinElmer TGA 4000 using ~10 ± 1 mg to maintain kinetic control. Independent repeat runs were not feasible post hoc due to limited access to the host facility and materials. Before each session, the balance was zeroed, gas lines were purged, and flow setpoints were verified. Runs were monitored for

baseline drift prior to heating; curves exhibiting abnormal buoyancy artifacts or excessive drift would be rejected (no runs were excluded). Samples were handled consistently (drying at 102°C for 36 h; milling/sieving to ≤ 180 μm) to minimize variability.

We report the sample mass tolerance (10 ± 1 mg), the total flow setpoint (100 mL min^{-1} with a nitrogen purge of 40 mL min^{-1}), and the temperature program (30°C–800°C at heating rates of 5, 10, and 20°C min^{-1}). Peak temperatures were obtained from the DTG maxima following peak deconvolution and used in the Kissinger analysis to estimate kinetic parameters.

Raw TGA/DTG files and processed datasets, as well as CHNS/XRF/ICP-MS outputs, can be made available on request from the corresponding author.

3. Results and Discussion

3.1. Characterization. Tables 1, 2, and 3 show the ultimate analysis, mineral composition measured using XRF, and mineral composition measured using ICP-MS of APS, respectively.

Using CHNS/HHV, XRF, and ICP-MS (Tables 1, 2, and 3), clear and base coats fall within typical carbon, hydrogen, and HHV ranges for viable pyrolysis feeds, whereas primer and electro have a very high mineral/ash (≈60 and ≈51 wt.%, respectively), diluting HHV and limiting convertible organics; phosphate is largely inorganic and energy-poor. High volatile matter implies a propensity for condensable vapors (tar) that can impair syngas quality unless mitigated [17]. Operationally, high ash burdens raise risks of slagging/fouling and can drive costs [18, 19]. The minerals identified by XRF/ICP-MS also include oxides, known to influence cracking (e.g., Al, Fe, Ca, and K), supporting a catalytic coprocessing role for ash-rich sludges.

Metal content in the APS streams can catalyze vapor cracking during pyrolysis, increasing H_2, CH_4 and other noncondensable gases [19]. Primer coat and electrocoat are therefore worth testing as binders with low-value biomass to boost thermal cracking. The phosphate coat, with 3% carbon by weight, an HHV of 0.611 MJ/kg, and ash above 70%, is not a suitable candidate for thermal decomposition; recovering metals or reusing it in construction as a cement or aggregate replacement is a more appropriate option.

Elemental data in Tables 2 and 3 show that APS sludges can act as catalysts in thermal treatment. Their mineral composition overlaps with that of major commercial catalysts, including zeolites and fluid cracking catalyst (FCC). Compounds such as SiO_2, Al_2O_3, K_2O, FeO, CaO, MgO, Na_2O_3, and Fe_2O_3 have been used to cut tar and improve bio-oil and syngas yields during gasification and pyrolysis of solid carbonaceous materials [20–26]. Because the APS streams differ in mineral composition, it would be beneficial to test copyrolysis and cogasification with other solid wastes to exploit potential synergies.

The base coat, with its high barium oxide content, could serve as an ethoxylation catalyst for reactions of ethylene oxide with alcohols. APS can also be calcined to produce ash suitable for use in catalysis. Prior work has demonstrated that ash content and composition significantly influence biomass pyrolysis and CO_2-gasification of waste tires [19, 27, 28]. Therefore, APS has clear potential for catalytic and synergistic use in the thermal treatment of carbonaceous materials.

Mineral profiles indicate that APS is a strong candidate for use in cement and concrete. All coats contain substantial amounts of aluminum, titanium, and calcium, while silicon is generally low, with the phosphate pretreatment stream being the only one showing appreciable silicon. XRF indicates that aluminum is present as alumina (Al_2O_3). In cement systems, silica and calcium oxide promote pozzolanic reactions, with alumina playing a supporting role [29]. Suitability as a cement paste additive will depend on how accessible these compounds are to the paste, for example, through factors such as fineness, solubility, and dispersion.

Table 1: Ultimate analysis of APS.

APS sample	N	C	H	S	O*	Ash	HHV (MJ/kg)
	wt.%						
Clear	5.21	54.70	8.09	0.00	27.16	4.84	26.57
Primer	1.52	22.81	2.79	4.62	8.02	60.24	9.88
Base	1.12	37.75	5.05	0.00	19.91	36.17	18.64
Electro	1.50	30.78	4.33	0.29	11.81	51.28	14.70
Phosphate	0.56	3.17	2.98	0.07	19.76	73.46	0.611

*Oxygen content is calculated by difference.

Table 2: Mineral composition of APS through XRF.

Elements (wt.%)	APS sample				
	Electro	Phosphate	Primer	Based	Clear
F	1.58	11.30	0	0	0
Na_2O	0	5.27	0.45	0	0.73
MgO	0.62	0.15	1.12	0.176	0.56
Al_2O_3	6.77	1.65	11.5	3.92	7.35
SiO_2	1.72	2.46	4.60	3.47	0.61
P_2O_5	19.20	22.2	0.62	0.53	0.11
SO_3	1.44	1.24	0.41	16.6	0.25
Cl	0.16	0.083	0.21	0.083	0.32
K_2O	1.79	3.70	0.20	0.032	0.030
CaO	4.66	1.27	0.62	0.68	1.49
TiO_2	5.12	0.13	51.80	21.40	0.088
Cr_2O_3	0.11	0.066	0.079	0.045	0.049
MnO	4.26	2.90	0.019	0.033	0
Fe_2O_3	6.96	15.60	1.63	0.35	0.27
NiO	3.14	1.80	0.12	0.014	0.013
CuO	0.19	0.0079	0.033	0.055	0.0081
Br	0.0042	0	0.0035	0	0.0020
ZnO	2.17	1.84	0.016	0.0107	0.016
SrO	0.026	0.0053	0.0078	0.51	0.0084
Y_2O_3	0	0.0013	0	0	0
ZrO_2	0.58	0.031	0.0147	0	0
BaO	0.90	0.022	0.18	40.70	0.032
Bi_2O_3	0.32	0.0094	0	0	0
CeO_2	0	0	0.25	0	0.091
Au	0	0	0.011	0	0
Co_3O_4	0	0	0.054	0	0
SnO_2	0	0	0.021	0	0

Table 3: Mineral composition of different automotive paint sludge samples using ICP-MS.

Elements (mg/kg)	APS sample				
	Clear	Based	Primer	Electro	Phosphate
Na	2523	323	1112	1465	6642
Mg	1232	255	1791	1126	201
Al	17,301	10,274	26,983	22,484	10,086
Si	688	526	961	658	7487.79
P	121	211	856	51,228	52,216
K	32	33	656	5382	23,049
Ca	2171	4339	1794	12,507	8266
Ti	18	106	238	88	3
Cr	65	109	199	192	185
Fe	459	887	4817	18,750	15,483
Ni	10	9	244	9243	3974
Cu	3	104	70	422	10
Br	3	9	22	35	3
Sr	25	1585	48	291	82
Zr	2	505	64	124	83
Cd	0.00	0.09	0.01	0.3	0.4
Te	0.00	0.00	0.00	0.03	0.05
Ba	277	22,973	1244	4796	181
Th	0.00	0.04	0.04	0.70	0.19

The high titanium oxide content in the primer coat also makes it a plausible candidate for ceramics, where titanium can improve color, durability, and thermal stability.

3.2. Decomposition Behavior of APS Sludge: TG-DTG. Figures 1 and 2 show the TG curves for four different APSs at heating rates of 5, 10, and 20°C/min under N_2 atmosphere and air atmosphere, respectively. The phosphate coat is excluded because of the very low volatile content.

At the same heating rate, mass loss scales with volatile content (clear coat > base coat > electrocoat > primer coat). Clear coat shows the fastest mass loss and strongest pyrolytic reactivity [30]. Relative to Figures 1 and 2, it shifts the main decomposition slightly higher in temperature and resolves two peaks more clearly across streams [5, 9, 30].

Stage 1 (30°C–200°C) shows small, smooth losses from moisture removal, below 6% of the initial mass, because the samples were predried. After this demoisturization period, Stage 2 starts above 220°C and accelerates to about 515°C in N_2 and about 550°C in air. Two distinct decomposition patterns are observed: from about 220°C to 380°C, release of VOCs and, in air, formation of H_2O and CO_2; and from about 380°C to 530°C, decomposition of resins and other high-boiling organics in the paint sludge[5].

Under the N_2 atmosphere, the two volatile fraction decomposition curves are only visible in clear coat sludge, which is a solvent based on melamine and acrylic [7]. The two peaks of volatile fraction decomposition are easily identifiable under the air atmosphere (Figure 2) for all paint sludges. The third and final weight loss stage starts from 515/530°C for the 2 atm, respectively, until the remainder of the temperature range. This stage is attributed to the carbonization and decomposition of inorganic components [9, 30] In Figure 1, for the N_2 atmosphere, a fourth stage can be

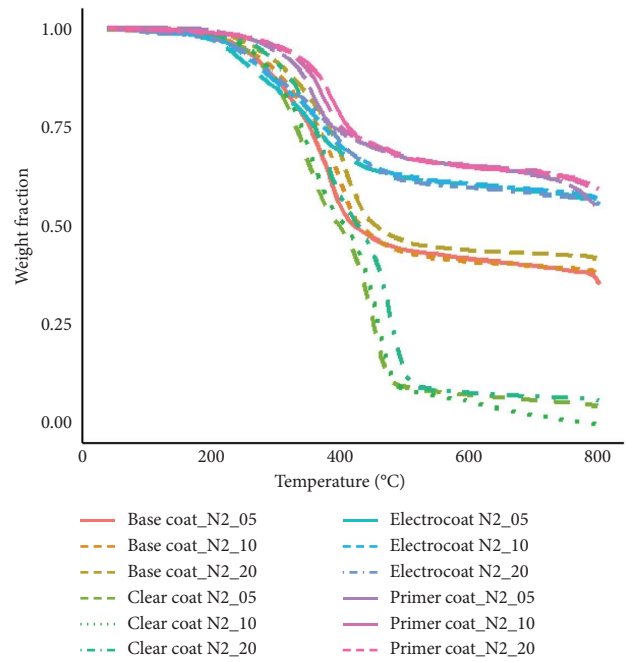

Figure 1: TG curves for different automated paint sludges at different heating rates under an N_2 atmosphere.

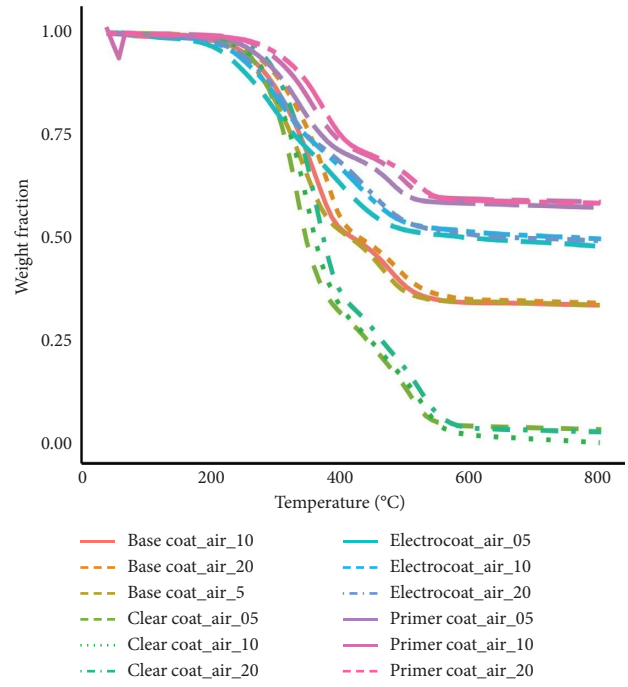

Figure 2: TG curves for different automated paint sludges at different heating rates under an air atmosphere.

observed at around 800°C, and this is because, at this point, the nitrogen purge gas was switched to air and held for 5 min to complete to ensure the complete combustion.

The thermogravimetric curve shows that much of the weight loss occurs during the second stage, which is known as the devolatilization stage. It is worth noting that the overall weight loss of primer sludge and electrocoat sludge is

very small at this stage for all heating rates tested, which is caused by the low volatile matter content and the high ash content in these two sludges. Equally, the fifth sludge, the phosphate coat, was not included on TG graphs due to only having a volatile matter content of 3 wt.%. Therefore, one would conclude that the only sludges that should be processed pyrolytically are the clear coat and base coat. Other sludges can find alternative re-uses in civil engineering applications and other material recovery processes. In a study by [9], which compared the decomposition behavior of sewage and paint sludge, it was concluded that the ash in paint sludge acts as a catalyst during the pyrolysis process. This, therefore, means that the components with higher ash composition would add synergistic benefits when copyrolyzed with other carbonaceous materials.

The three-step process of weight loss corresponds to the three peaks observed in the DTG curves, Figures 3 and 4. The first peak is small and corresponds to the demoisturization of the sample [31]. There is a significant turning point in the TG curve that divides the devolatilization stage into two stages, and this corresponds to the two major peaks observed on the DTG curve. Figures 1, 2, 3, and 4 show the three different heating rates and the 2 atm studied. Increasing the heating rate shifts the weight loss peak of the sample from a low to a high temperature zone, and this has been attributed mainly to the influence of heat transfer between the sample particles and inside the particles. A larger temperature gradient exists at higher heating rates, which causes the pyrolysis of internal components to lag [30]. The influence of oxygen can be noticed when comparing the pyrolysis DTG curves under N_2 (Figure 3) and air (Figure 4). The oxidation of the volatiles and char shifted the two peaks to lower temperatures [32].

3.3. Pyrolysis Reaction Kinetics

3.3.1. Approach. To determine the activation energy (E_a) and pre-exponential factor (K_0) of the thermal decomposition processes determined with the sludges studied, we designed an original and automated procedure using MATLAB software. The procedure is based on the Kissinger method. This approach is widely used in thermal analysis because it provides a straightforward way to extract kinetic parameters from nonisothermal experiments without requiring knowledge of the reaction progress (α). The thermal decomposition was studied using TGA, and the kinetic parameters were obtained from the derivative of the weight loss curve (Figures 3 and 4). To deconvolute overlapping decomposition processes, the program uses the peakfit function in MATLAB. This function fits multiple peaks to the DTG curve and extracts the relevant peak parameters, such as

- Mean decomposition temperature (T_m): Corresponds to the peak position of each deconvoluted reaction.

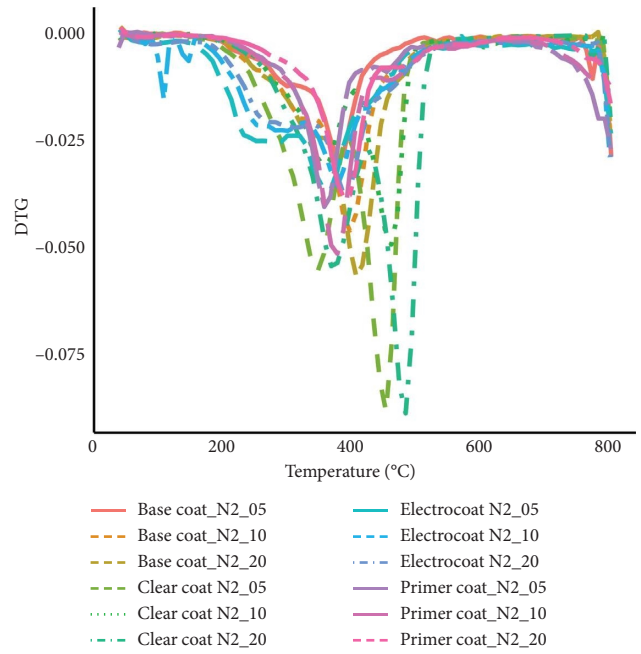

Figure 3: DTG curves of APS under an inert nitrogen gas environment.

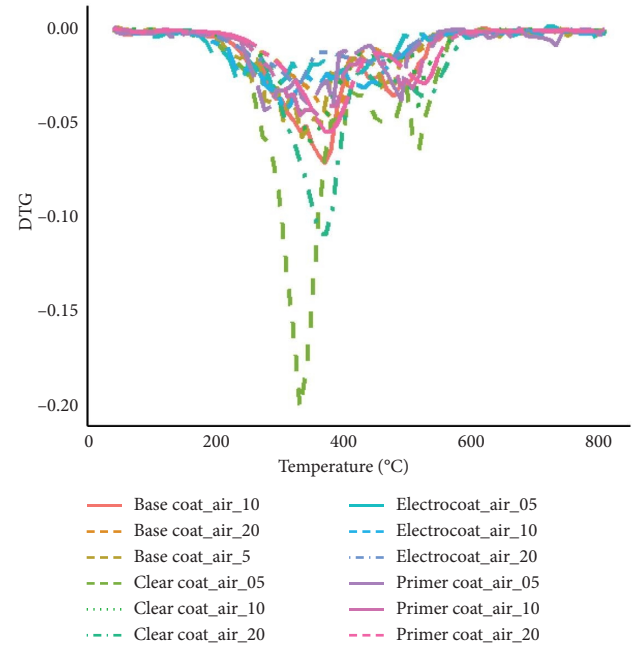

Figure 4: DTG curves of APS under an air atmosphere.

- Peak amplitude (ΔT): Represents the intensity of each thermal event, helping to distinguish between different decomposition steps.

Two fractions were necessary to correctly fit the data for the decomposition of the materials considered. The extracted T_m values of the two peaks were then used in the Kissinger analysis. This would represent the decomposition

of each material by the sum of two different fractions decomposing simultaneously as

$$\text{fraction } 1 \xrightarrow{k_{01},\, E_1} \text{volatiles } 1 + \text{solid } 1, \tag{1}$$

$$\text{fraction } 2 \xrightarrow{k_{02},\, E_2} \text{volatiles } 2 + \text{solid } 2. \tag{2}$$

The initial relative weight of each fraction (f_{10} and f_{20}) can also be determined. Obviously, the sum of these two fractions would be unity.

For example, in the case of clear coat decomposed in nitrogen atmosphere at 20 K/min, we obtained Figure 5.

As we can check, the deconvolution of the experimental derivative (dots in the previous figure) into two different fractions (green lines) is quite cogent. In this case, as shown in the figure, we obtained the following:

- Mean decomposition temperature of the first process: 640.8 K.
- Peak amplitude of the first process: 127.7 K.
- Mean decomposition temperature of the second process: 748.2 K.
- Peak amplitude of the second process: 42.2 K.

The "peakfit" function also calculates the areas of the corresponding processes. The initial weights of each fraction (f_{10} and f_{20}) are estimated from the area data, as the quotient of each area divided by the sum of areas.

The Kissinger equation is based on the Arrhenius equation and is given by

$$\ln\left(\frac{\beta}{T_m^2}\right) = -\frac{E_a}{RT_m} + C, \tag{3}$$

where

- β is the heating rate (K/min).
- T_m is the mean process temperature (K), extracted using peakfit.
- E_a is the activation energy (J/mol).
- R is the universal gas constant (8.314 J/mol·K).
- C is a constant.

By plotting $\ln(\beta/T_m^2)$ vs. $1/T_{m1}$ for the different heating rates used in the runs, and fitting a linear regression, we obtained the slope as

$$\text{slope} = \frac{-E_a}{R}. \tag{4}$$

Once E_a was determined, we used the rearranged Arrhenius equation as

$$K_0 = \frac{\beta E_a}{R T_m^2} \cdot e^{\left((E_a)/(RT_m)\right)}. \tag{5}$$

This formula was applied to compute pre-exponential factors for each heating rate, and an average value was obtained. For example, Figure 6 shows the Kissinger's plot for the case of electrocoat in a nitrogen atmosphere. Similar plots were performed for all materials, and once all the data were processed, key kinetic parameters were extracted and can be found in Table 4.

The data in Table 4 can be conveniently plotted in a graph showing the temperature interval where the reaction takes place and the corresponding activation energy. Figure 7 shows the activation energies of the decomposition of each material in the temperature interval where each reaction takes place in both atmospheres.

The computed activation energies (E_a) and pre-exponential factors (K_0) were analyzed to ensure that they were within reasonable ranges for thermal decomposition reactions (typically 50–250 kJ/mol). The order of reaction (n) was not explicitly determined, as the Kissinger method assumes $n = 1$ implicitly. The Kissinger method provided an effective way to estimate the kinetic parameters of the thermal decomposition processes. The use of the peakfit function allowed for an accurate extraction of T_m values from complex DTG curves, enabling a reliable estimation of E_a and k_0. These parameters can now be used to model the reaction kinetics and predict thermal behavior at different heating rates.

3.3.2. Observation. The kinetic parameters (E_a and k_0) derived for the APSs provide a crucial quantitative foundation for process design. Placing these values in the context of other well-studied waste streams reveals the unique challenges and opportunities presented by APS.

The E_a values for APS are not monolithic and denote diverse material composition as follows:

1. Clear and base coats (pyrolysis E_a: 126–140 kJ/mol): These values fall within the upper range typical for lignocellulosic biomass (e.g., wood and agricultural residues), which generally exhibits E_a between 50 and 150 kJ/mol for primary devolatilization. This suggests that the energy input required to pyrolyze these paint streams is similar to that for conventional biomass.
2. Primer and electrocoat (pyrolysis E_a: 74–100 kJ/mol): These significantly lower values are more akin to those reported for sewage sludge. This is a strong indicator that the high inorganic content (ash > 50%) in these streams is not inert. Compounds such as TiO_2 in the primer and P_2O_5/NiO in the electrocoat likely act as catalysts, lowering the apparent energy barrier for decomposition.
3. Second-stage decomposition (pyrolysis E_a up to 203 kJ/mol): The very high E_a for the second stage of clear and base coats is notable. It exceeds the activation energies commonly reported for many plastics such as polypropylene (~150–200 kJ/mol) and approaches that of polyethylene. This indicates that the cross-linked, cured paint resins form highly stable chemical structures or char intermediates that are difficult to break down.

These comparisons lead to direct engineering implications. The high E_a values for key stages mean that pyrolysis

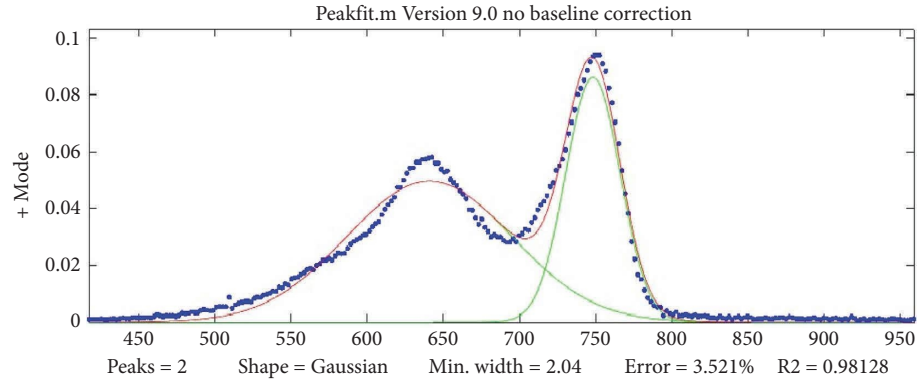

FIGURE 5: Deconvolution performed by the "peakfit" function with the data of the derivative with respect to temperature of the run performed at 20 K/min using clear coat, as an example of the procedure followed.

TABLE 4: Kinetic parameters for the decomposition of each material, both in nitrogen (pyrolysis) and air (combustion).

		Log (k_{01} [s^{-1}])	E_1 (kJ/mol)	Log (k_{02} [s^{-1}])	E_2 (kJ/mol)	f_{01}	T_{m1}	ΔT_1	T_{m2}	ΔT_2
Pyrolysis	Clear coat	4.18	125.8	5.68	170.3	0.64	640.8	127.7	748.2	42.3
	Base coat	5.02	139.5	9.96	202.5	0.37	655.2	50.6	658.3	245.5
	Primer coat	−0.28	73.7	−5.71	10.8	0.97	661.8	132.6	870.6	104.9
	Electrocoat	3.90	99.7	3.59	121.7	0.29	530.1	92.7	654.8	134.5
Combustion	Clear coat	8.50	173.0	8.19	215.7	0.71	619.5	90.6	771.5	105.8
	Base coat	4.30	125.2	6.53	190.3	0.75	631.1	109.3	777.5	66.0
	Primer coat	4.78	129.9	8.84	220.1	0.83	625.6	116.5	763.3	66.6
	Electrocoat	5.31	124.8	4.28	143.6	0.61	572.1	117.1	714.8	104.2

Note: values of mean decomposition temperatures and peak amplitudes for the different materials are presented.

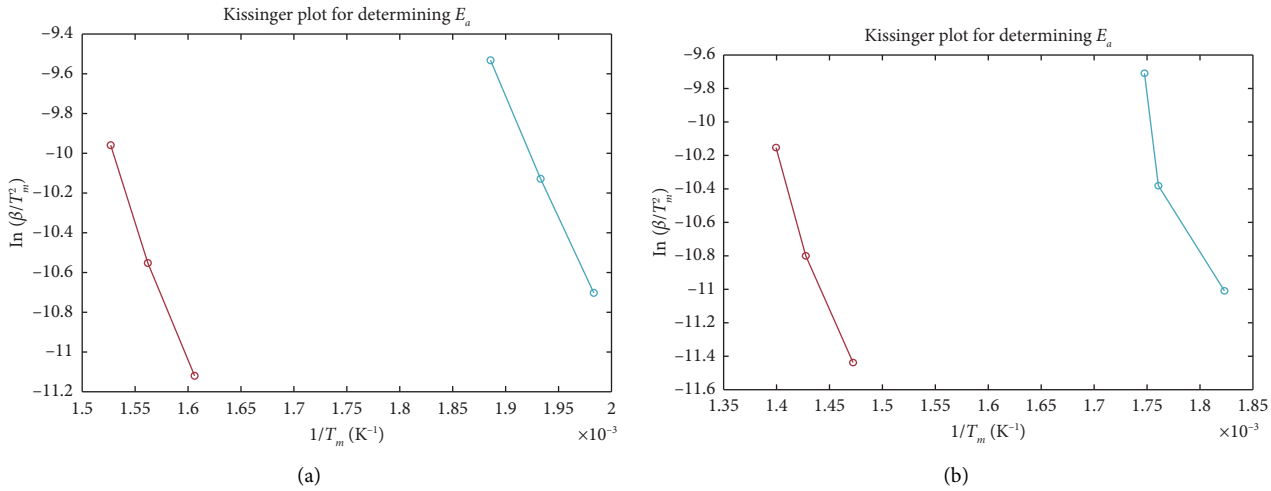

FIGURE 6: Kissinger plot for the pyrolysis (a) and the combustion (b) of electrocoat.

or gasification processes cannot be run at the lower end of typical temperature ranges (400°C–500°C). To achieve complete conversion and minimize tar, higher temperatures or longer solid residence times are likely necessary, impacting reactor design and energy balance. The low E_a of ash-rich streams such as primer and electrocoat is a potential advantage. In cogasification or copyrolysis with other wastes (e.g., biomass and plastics), these streams could serve as an in situ catalyst, promoting tar cracking and improving gas quality without the cost of an external catalyst.

The kinetic data solidify the conclusion that APS cannot be treated as a single feedstock. Clear and base coats are suitable for energy-focused pyrolysis. In contrast, the ash-rich primer and electrocoat are better candidates for catalytic

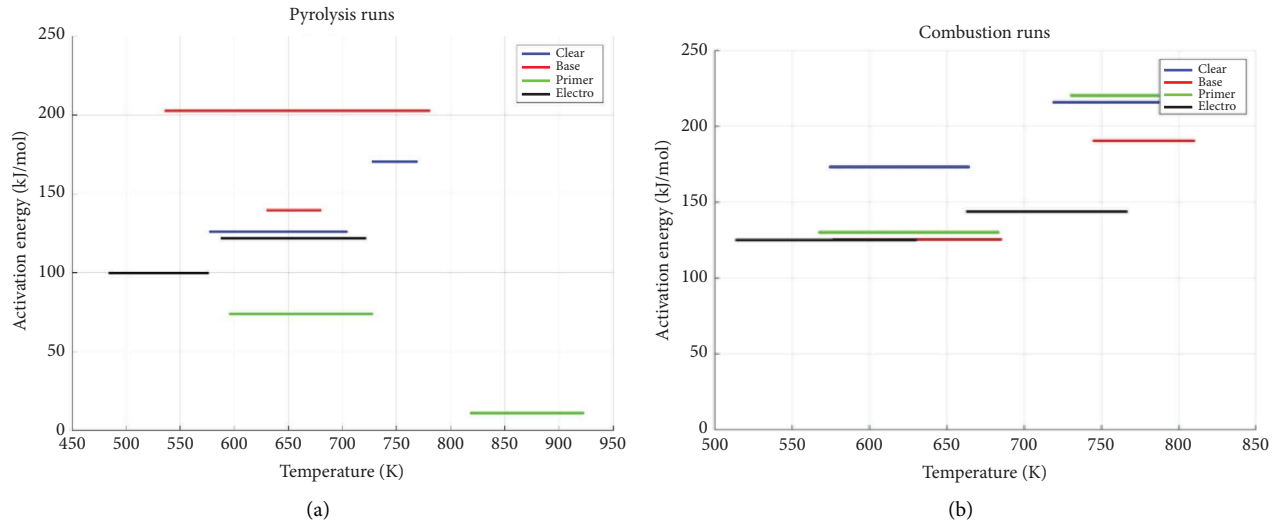

FIGURE 7: Activation energies of the decomposition of each material, both in nitrogen (a) and air (b). The *X*-axis represents the temperature interval where each reaction takes place.

coprocessing or material recovery (e.g., in cement), where their minerals add value rather than pose a disposal problem.

4. Conclusion

The results elucidate the decomposition of APSs in N_2 and in air at 5°C–20°C/min and show three clear stages: moisture removal at 30°C–200°C; devolatilization and resin breakdown from about 220°C to roughly 515°C in N_2 and about 550°C in air, often in two substeps; and, at higher temperature, carbonization with changes in inorganic phases. Mass loss follows volatile content, with the clear coat having the highest and the primer the lowest, consistent with stream composition. These patterns translate into practical routes. Clear coat and base coat are suitable candidates for pyrolysis aimed at oil and gas recovery, with operating windows chosen around the two devolatilization substeps. Primer coat, electrocoat, and phosphate streams are better directed to mineral recovery or to civil engineering uses such as cement or aggregate replacement; their calcined ash may also serve as a catalyst in thermal treatments. Coprocessing remains attractive, where catalytic minerals can assist cracking, but should be matched to the composition of each stream. Kinetic parameters indicate no intrinsic kinetic barrier within the tested temperature ranges and heating rates, so kinetics are unlikely to be the primary constraint on cogasification. In summary, the kinetic analysis shows that APS thermoconversion sits at the intersection of biomass and plastic pyrolysis, with the added complexity of intrinsic catalytic minerals. A successful design must be tailored to the specific sludge stream, leveraging its unique kinetic signature to optimize temperature, residence time, and coprocessing partners. That said, scale-up can be limited by heat and mass transfer, feed variability, ash sintering or slagging, and emission control. Pilot-scale trials should confirm residence times, heat input, and gas–solid contact before full deployment. Prior to process scale-up, further investigations using an integrated pyrolysis with mass spectrometric analysis are necessary to comprehensively characterize the composition and distribution of the volatile compounds released during the thermochemical treatment of APS. Overall, the study provides stream-level guidance on temperature ranges, residence times, expected oil and gas yields, and likely emission precursors to support process selection.

Data Availability Statement

Data will be made available on request to the corresponding author.

Conflicts of Interest

The authors declare no conflicts of interest.

Funding

The research was supported by the National Research Foundation of South Africa through the NRF Transformation Award grant (NSTA231113163202).

Acknowledgments

The authors would like to acknowledge the University of South Africa, the University of Alicante, and the VW Group South Africa for their respective support.

References

[1] P. Lisbona, S. Pascual, and V. Pérez, "Waste to Energy: Trends and Perspectives," *Chemical Engineering Journal Advances* 14 (2023): 100494, https://doi.org/10.1016/j.ceja.2023.100494.

[2] A. O. Omotayo, "Investigating the Drivers of Solid Waste Generation and Disposal: Evidence From South Africa," *Environment, Development and Sustainability* (2024): https://doi.org/10.1007/s10668-024-04987-7.

[3] Z. Liu, Z. Huang, Y. Yan, et al., "Characterizing the Emission Behaviors of Cumulative VOCs From Automotive Solvent-Based Paint Sludge," *Journal of Environmental Management* 317 (2022): 115369, https://doi.org/10.1016/j.jenvman.2022.115369.

[4] Z. Liu, Y. Yan, T. Lv, et al., "Comprehensive Understanding the Emission Characteristics and Kinetics of VOCs From Automotive Waste Paint Sludge in a Environmental Test Chamber," *Journal of Hazardous Materials* 429 (2022): 128387, https://doi.org/10.1016/j.jhazmat.2022.128387.

[5] L. Tian, T. Liu, J. Yang, et al., "Pyrolytic Kinetics, Reaction Mechanisms and Gas Emissions of Waste Automotive Paint Sludge via TG-FTIR and Py-GC/MS," *Journal of Environmental Management* 328 (2023): 116962, https://doi.org/10.1016/j.jenvman.2022.116962.

[6] B. Ruffino, G. Campo, S. S. Idris, G. Salihoğlu, and M. Zanetti, "Automotive Paint Sludge: A Review of Pretreatments and Recovery Options," *Resources* 12, no. 4 (2023): 45, https://doi.org/10.3390/resources12040045.

[7] G. Salihoglu and N. K. Salihoglu, "A Review on Paint Sludge From Automotive Industries: Generation, Characteristics and Management," *Journal of Environmental Management* 169 (2016): 223–235, https://doi.org/10.1016/j.jenvman.2015.12.039.

[8] S. S. Idris, M. N. Bojy, and Z. Januri, "Conversion of Automotive Paint Sludge to Activated Carbon via Microwave Pyrolysis Technique for Supercapacitor Application," *Malaysian Journal of Chemical Engineering and Technology* 3, no. 1 (2020): 35–43, https://doi.org/10.24191/mjcet.v3i1.11234.

[9] A. Zhou, N. Deng, S. Deng, et al., "Study on Pyrolysis Behavior of Municipal Sludge Based on TG-FTIR-MS," *Journal of the Energy Institute* 114 (2024): 101643, https://doi.org/10.1016/j.joei.2024.101643.

[10] N. F. Abu Bakar, M. N. Muhd Sidek, S. M. Suharman, and N. Abd Rahman, "Characterization and Evaluation of Dried Automotive Paint Sludge as Cement-Based Composite," *Materials Today: Proceedings* 63 (2022): S301–S305, https://doi.org/10.1016/j.matpr.2022.03.151.

[11] B. C. Burande, "Utilisation of Paint Sludge From Automotive Industries Into Valuable Products," *International Journal of Recent Trends in Engineering and Research* 3 (2017): 513–519, https://doi.org/10.23883/ijrter.2017.3257.rpnmg.

[12] S. Li, J. Feng, S. Tian, et al., "Tuning Role and Mechanism of Paint Sludge for Characteristics of Sewage Sludge Carbon: Paint Sludge as a New Macro-Pores Forming Agent," *Journal of Hazardous Materials* 344 (2018): 657–668, https://doi.org/10.1016/j.jhazmat.2017.11.012.

[13] A. E. Mavukwana, N. Stacey, J. A. Fox, and B. C. Sempuga, "Thermodynamic Comparison of Pyrolysis and Gasification of Waste Tyres," *Journal of Environmental Chemical Engineering* 9, no. 2 (2021): 105163, https://doi.org/10.1016/j.jece.2021.105163.

[14] K. R. Goud Burra, I. F. Hernández, M. J. Castaldi, A. Mavukwana, and A. K. Gupta, "Gasification of Municipal Solid Wastes With Gypsum Wastes Under Different Gasifying Environments," *Journal of the Energy Institute* 114 (2024): 101644, https://doi.org/10.1016/j.joei.2024.101644.

[15] I. Oliver, J. A. Conesa, and A. Fullana, "Thermal Decomposition of Bio-Based Plastic Materials," *Molecules* 29, no. 13 (2024): 3195, https://doi.org/10.3390/molecules29133195.

[16] K. Al-Qayim, W. Nimmo, K. Hughes, and M. Pourkashanian, "Kinetic Parameters of the Intrinsic Reactivity of Woody Biomass and Coal Chars via Thermogravimetric Analysis," *Fuel* 210 (2017): 811–825, https://doi.org/10.1016/j.fuel.2017.09.010.

[17] J. O. Ajikashile, M. Alhnidi, M. Bishir, and A. Kruse, "The Influence of Torrefaction Temperature and Reaction Time on the Properties of Torrefied Sun-Dried Millet and Sorghum Straws From the Arid and Semi-Arid Zones of Western Africa," *Biofuels, Bioproducts and Biorefining* 17, no. 3 (2023): 751–767, https://doi.org/10.1002/bbb.2464.

[18] K. Głód, J. Lasek, K. Słowik, et al., "Investigation of Ash-Related Issues During Combustion of Maize Straw and Wood Biomass Blends in Lab-Scale Bubbling Fluidized Bed Reactor," *Journal of Energy Resources Technology, Transactions of the ASME* 142 (2020): 1–11, https://doi.org/10.1115/1.4044221.

[19] L. Puri, Y. Hu, and G. Naterer, "Critical Review of the Role of Ash Content and Composition in Biomass Pyrolysis," *Frontiers in Fuels* 2 (2024): 1378361–19, https://doi.org/10.3389/ffuel.2024.1378361.

[20] M. Arabiourrutia, G. Lopez, M. Artetxe, J. Alvarez, J. Bilbao, and M. Olazar, "Waste Tyre Valorization by Catalytic Pyrolysis–A Review," *Renewable and Sustainable Energy Reviews* 129 (2020): 109932, https://doi.org/10.1016/j.rser.2020.109932.

[21] P. K. Kanduri and S. Seethamraju, "In Situ and Ex Situ Catalytic Co-Pyrolysis of Lignocellulosic Biomass and Plastics (Low-Density and High-Density Polyethylene) Using Spent FCC Catalyst," *Waste and Biomass Valorization* 14, no. 5 (2022): 1737–1751, https://doi.org/10.1007/s12649-022-01961-0.

[22] U. Khalil, J. Vongsvivut, M. Shahabuddin, S. P. Samudrala, S. C. Srivatsa, and S. Bhattacharya, "A Study on the Performance of Coke Resistive Cerium Modified Zeolite Y Catalyst for the Pyrolysis of Scrap Tyres in a Two-Stage Fixed Bed Reactor," *Waste Management* 102 (2020): 139–148, https://doi.org/10.1016/j.wasman.2019.10.029.

[23] J. Ren, J.-P. Cao, X.-Y. Zhao, F.-L. Yang, and X.-Y. Wei, "Recent Advances in Syngas Production From Biomass Catalytic Gasification: A Critical Review on Reactors, Catalysts, Catalytic Mechanisms and Mathematical Models," *Renewable and Sustainable Energy Reviews* 116 (2019): 109426, https://doi.org/10.1016/j.rser.2019.109426.

[24] A. O. Odjo, A. N. García, and A. Marcilla, "Refinery Nonconventional Feedstocks: Influence of the Coprocessing of Vacuum Gas Oil and Low Density Polyethylene in Fluid Catalytic Cracking Unit on Full Range Gasoline Composition," *Energy & Fuels* 28, no. 2 (2014): 1579–1593, https://doi.org/10.1021/ef4020394.

[25] I. Samprón, L. F. de Diego, F. García-Labiano, M. T. Izquierdo, A. Abad, and J. Adánez, "Biomass Chemical Looping Gasification of Pine Wood Using a Synthetic Fe_2O_3/Al_2O_3 Oxygen Carrier in a Continuous Unit," *Bioresource Technology* 316 (2020): 123908, https://doi.org/10.1016/j.biortech.2020.123908.

[26] S. Varjani, "Efficient Removal of Tar Employing Dolomite Catalyst in Gasification: Challenges and Opportunities," *Science of the Total Environment* 836 (2022): 155721, https://doi.org/10.1016/j.scitotenv.2022.155721.

[27] S.-H. Cho, J.-I. Oh, S. Jung, et al., "Catalytic Pyrolytic Platform for Scrap Tires Using CO_2 and Steel Slag," *Applied Energy* 259 (2020): 114164, https://doi.org/10.1016/j.apenergy.2019.114164.

[28] G. Czerski, K. Śpiewak, P. Grzywacz, and F. Wierońska-Wiśniewska, "Assessment of the Catalytic Effect of Various Biomass Ashes on CO_2 Gasification of Tire Char,"

Journal of the Energy Institute 99 (2021): 170–177, https://doi.org/10.1016/j.joei.2021.09.003.

[29] E. C. Tsardaka, K. Sougioultzi, A. Konstantinidis, and M. Stefanidou, "Interpreting the Setting Time of Cement Pastes for Modelling Mechanical Properties," *Case Studies in Construction Materials* 19 (2023): e02364, https://doi.org/10.1016/j.cscm.2023.e02364.

[30] S. Zhou, Q. Zhao, T. Yu, and X. Yao, "Co-Pyrolysis of Sewage Sludge With Paint Sludge: Kinetics and Thermodynamic Analysis via Iso-conversional Methods," *Journal of Wuhan University of Technology-Materials Science Edition* 39, no. 3 (2024): 716–727, https://doi.org/10.1007/s11595-024-2930-6.

[31] P. Fu, S. Hu, J. Xiang, L. Sun, S. Su, and S. An, "Study on the Gas Evolution and Char Structural Change During Pyrolysis of Cotton Stalk," *Journal of Analytical and Applied Pyrolysis* 97 (2012): 130–136, https://doi.org/10.1016/j.jaap.2012.05.012.

[32] A. Magdziarz and S. Werle, "Analysis of the Combustion and Pyrolysis of Dried Sewage Sludge by TGA and MS," *Waste Management* 34, no. 1 (2014): 174–179, https://doi.org/10.1016/j.wasman.2013.10.033.